ROYAL SOCIETY
OF CHEMISTRY

PAPER

Check for updates

A red emitting carbon dot and aptamer-functionalized alginate system for targeted triple-negative breast cancer imaging

Simone Maturi,[a] Alessandra Caliendo, [ID] [b] Silvia Tortorella, [ID] [a] Nina Kostevšek, [ID] [c,d] Erica Locatelli, [ID] [a] Mauro Comes Franchini, [ID] [a] Lisa Agnello,[b] Simona Camorani, [ID] [b] Laura Cerchia [ID] *[b] and Letizia Sambri [ID] *[a]

The targeted detection of cancer cells is crucial for tumour diagnosis and therapeutic treatment. Recently, luminescent carbon dots have generated wide interest in biomedical applications, thanks to their unique properties such as biocompatibility, tuneable emission, water solubility and the possibility of surface functionalization. Herein, we report the conjugation of red emitting carbon dots (**RCDs**) to alginate and the **sTN58** aptamer to obtain systems able to selectively recognize cancer cells that can be exploited in bioimaging and potentially as photothermal agents.

Introduction

Cancer represents a major health issue with a high mortality rate worldwide, and according to the WHO, it accounted for nearly 10 million deaths in 2020.[1] Therefore, the development of new and effective strategies for cancer diagnosis and treatment is still urgent.

The targeted detection and imaging of tumour cells is crucial for cancer diagnosis and potential therapeutic treatment. However, common imaging agents suffer from various limitations, such as poor biocompatibility, inadequate optical properties in the light therapeutic window and lack of stability.[2] Recent advances in synthetic techniques have allowed exploring promising nanoparticles, as luminescent carbon dots (CDs) and their derivatives, in biomedical imaging. In fact, CDs are 0-dimensional luminescent carbon nanomaterials that since their fortuitous discovery in 2004[3] have found widespread use in several fields such as bioimaging, nanomedicine, chemical- and bio-sensing, drug delivery and cancer therapy.[4–6] This is because they possess unique properties, such as bright tuneable fluorescence, high photo-

stability, biocompatibility, water solubility and the presence of functional groups on their surface that permit their further derivatization and modification.[7,8] In addition, bottom-up synthetic approaches that employ small renewable organic molecules, or also bio-waste, make CDs environmentally friendly and cost-effective nanoparticles.[9,10]

In particular, red emitting carbon dots (**RCDs**) exhibiting good optical properties in the therapeutic window present huge advantages over blue- and green-emitting ones for biological applications, thanks to their deep tissue penetration, low autofluorescence and high image contrast, so that their employment in bioimaging and phototherapy is currently developing very fast.[11] The use of nitrogen-containing starting materials led to a shift in the emission of the synthesized CDs towards the red and near infra-red regions, as reported in various recent papers.[12,13]

Besides the luminescence properties, one of the major advantages of CDs is the possibility of conjugating them to different molecules through the formation of covalent bonds with the functional groups, like carboxylic acids or amino groups, present on their surface. Therefore, with the aim of exploiting our recently obtained **RCDs**[14] as luminescent probes in bioimaging, we designed their coordination to a system able to selectively recognize cancer cells.

Alginate (**Alg**) is an anionic natural biopolymer, a linear polysaccharide consisting of α-ʟ-guluronic acid (G) and β-ᴅ-mannuronic acid (M) units, linked by 1,4-glycosidic linkages. Obtained mainly from brown seaweeds, it recently received remarkable attention due to its versatile properties, such as biocompatibility, biodegradability and the possibility of chemical modification of its functional groups; thanks to these pro-

[a]*Department of Industrial Chemistry "Toso Montanari", University of Bologna, Via Piero Gobetti 85, 40129 Bologna, Italy. E-mail: letizia.sambri@unibo.it*
[b]*Institute of Endotypes in Oncology, Metabolism and Immunology "Gaetano Salvatore", National Research Council, 80131 Naples, Italy. E-mail: laura.cerchia@cnr.it*
[c]*Department for Nanostructured Materials, Jožef Stefan Institute, Jamova 39, 1000 Ljubljana, Slovenia*
[d]*Jožef Stefan International Postgraduate School, Jamova 39, 1000 Ljubljana, Slovenia*

perties, alginate has been employed in a wide range of applications in biomedicine, from gel formation to tissue engineering and drug delivery.[15–18]

Oligonucleotide aptamers represent a striking alternative to peptides and antibodies as cancer-targeting recognition elements, owing to their advantageous chemical synthesis, which allows for cost-effective, time-efficient production with high reproducibility.[19] Additionally, aptamers are amenable to a wide range of chemical modifications to enhance their half-lives, reduce toxicity, and enable conjugation with diverse therapeutic and/or diagnostic nanoformulations.[20]

Triple-negative breast cancer (TNBC) is a subtype of breast cancer with the least favourable outcome due to tumour heterogeneity, limited targeted therapy options and resistance to standard chemotherapeutic regimens.[21] In a previous work,[22] we developed the neutralizing anti-CD44 2′fluoro-pyrimidines (2′F-Pys)-containing RNA aptamer **sTN58**, which demonstrates exceptional targeting efficacy across multiple TNBC cell lines and clinical patient-derived samples. This aptamer exhibits high binding affinity toward chemoresistant cell populations and possesses several features relevant for active tumour targeting, including high binding affinity and specificity, efficient cellular internalization, elevated serum stability, rapid and high tumour accumulation, and a favourable safety profile with no systemic toxicity. Moreover, **sTN58** acts effectively as a targeting ligand for the delivery of doped conjugated polymer nanoparticles to TNBC cells, enabling their selective photoeradication.[23]

With the above background in mind, we chose to functionalize[24] **Alg** with **RCDs** and the **sTN58** aptamer to obtain new powerful systems to be applied as fluorescent probes in targeted bioimaging of TNBC cells.

In addition to imaging capacity, we evaluated the therapeutic potential of our system as well. PTT (photothermal therapy) is an effective method that takes advantage of the ability of specific systems to efficiently convert light energy into heat to kill cancer cells.[25] PTT has received widespread attention because it is minimally invasive, and it can be combined with other treatments to increase the success rate.[26] Among the desirable requirements to work usefully as photothermal agents, these systems should absorb at long wavelengths, together with being nontoxic and able to target cancer cells.[27] Although **RCDs** have recently been exploited as photothermal agents in cancer therapy,[27] advanced surface engineering of **RCDs** for the purpose of active targeting in combination with PTT remains rarely described. Therefore, some preliminary experiments were performed regarding the photothermal activity of the obtained systems, indicating their great potential for use in combinatorial therapy.

Materials and methods

A TEM FEI TECNAI F20 transmission electron microscope operating at 200 keV was utilized to obtain high-resolution transmission electron microscopy (TEM) images. The ultra-violet–visible (UV–vis) absorption spectra were recorded using a Cary UV-vis spectrometer. The fluorescence spectra were recorded using an Edinburgh FLSP920 spectrometer equipped with a 450 W xenon arc lamp, double excitation and single emission monochromators, and a Peltier-cooled Hamamatsu R928P photomultiplier tube (185–850 nm) spectrofluorometer. The FT-IR spectra were recorded using a PerkinElmer Spectrum 2000 FT-IR spectrometer. Z-potential measurements were performed using a Malvern Instruments – Zetasizer Nano ZS with the samples placed in disposable folded capillary cells in distilled water solution. Photothermal experiments were performed using an FC-808 fiber coupled laser system (CNI Optoelectronics Tech) in the continuous-wave operation mode at 808 nm with different laser powers.

Chemicals and aptamers

Citric acid 99%, alginic acid sodium salt and N-ethyl-N'-(3-dimethylaminopropil)carbodiimide (EDC) have been purchased from Sigma-Aldrich; spermidine was provided by Acros Organics; formamide and N-hydroxysuccinimide (NHS) were provided by VWR. Acetone and ethanol (analytical grade) and dichloromethane (DCM, GC grade, ≥99.8%) were obtained from Sigma-Aldrich. All the reagents and the solvents were used without any further purification.

NH$_2$-terminated 2′F-Pys-containing RNA sTN58 and non-related scrambled (SCR) aptamers were synthesized by LGC Biosearch Technologies (Risskov, Denmark).

sTN58: 5′ (NH2-C6) GGACAUAUGAUGCAACGUUGUGGUC CCGUUUGCACUUUGUUUACG3′.

SCR: 5′ (NH2-C6) UUCGUACCGGGUAGGUUGGCUUGCAC AUAGAACGUGUCA3′.

Synthesis and purification of RCDs

Citric acid (300 mg, 1.56 mmol) was solubilized in formamide (20 mL) under stirring with a magnetic stir-bar at room temperature in a Teflon chamber of a stainless autoclave. After complete solubilization, spermidine (1.1 g, 7.57 mmol) was added to the solution and stirred until complete dissolution. The Teflon chamber was then sealed inside the stainless autoclave, covered with aluminium foil, placed on a magnetic stirrer and heated at 190 °C for 4 hours under stirring (400–600 rpm). At the end of the reaction, the heating was turned off and the autoclave was allowed to cool to room temperature overnight. The autoclave was then opened and the solution in the Teflon chamber was purified by filtering it through a syringe equipped with a 0.22 μm Sterivex and dripped into a beaker with 200 mL of acetone. The resulting suspension was centrifuged using Falcon tubes at 9000 rpm for 20 minutes, and then the surfactant was discarded while the precipitate was washed with a 1 : 1 acetone : EtOH solution and centrifuged with the same parameters as before. Once more the surfactant was discarded and the solid was recovered using DCM and collected into a pear-shaped flask and was allowed to decant for several hours. The solvent was then removed from the top of the flask and the solid was then dried under reduced pressure to obtain around 220 mg (73% yield determined in relation to

the initial amount of citric acid) of a red-brownish powder of **RCDs** that was stored in a capped vial.

Synthesis and purification of RCDs@Alg

Previously synthesized **RCDs** (80 mg) were dissolved in 10 mL of distilled water. At the same time, alginic acid sodium salt (530 mg) was dissolved in a 100 mL round bottom flask equipped with a stir-bar under strong stirring; then, a solution of EDC (530 mg, 3.42 mmol) in 10 mL of distilled water was added to the sodium alginate solution and the mixture was left to react for about 10 minutes. At this point, the **RCD** solution previously prepared was added to the sodium alginate–EDC solution, the flask was sealed, and the system was allowed to react overnight at room temperature under stirring.

The solution was then transferred into a 3500 MWCO dialysis membrane and dialyzed against distilled water for 3 days. After 24 hours of dialysis, a dark reddish solution was recovered in a round bottom flask, sealed and stored in a fridge.

Synthesis and purification of RCDs@Alg@sTN58 and RCDs@Alg@SCR

A solution of **RCDs@Alg** (1.30 mL, dry matter: 6.5 mg mL^{-1}) was placed in a vial equipped with a magnetic stirrer; then, a solution of EDC (280 mM, 2 mL) was added, and the system was allowed to react for 10 minutes. Then, a solution of NHS (2.3 mM, 1 mL) was added, and the system was allowed to react for 5 minutes. Meanwhile, the aptamers **sTN58** and **SCR** (133 pmol μL^{-1}, 1 μL) were diluted up to 1 mL and heated at 85 °C for 5 minutes, and then cooled in ice for 2 minutes and heated at 37 °C for 10 minutes. Then, the solutions were added into the **RCDs@Alg** solution, left under stirring at 37 °C overnight and dialyzed for 24 hours in the 3500 MWCO dialysis membrane against distilled water. The resulting reddish **RCDs@Alg@sTN58** and **RCDs@Alg@SCR** solutions were then recovered and stored in a sealed vial in the fridge. To determine the amount of aptamer conjugated to **RCDs@Alg**, a reverse transcription-quantitative polymerase chain reaction (RT-qPCR) based assay was performed as previously described.[28–30] The quantity of the amplified product was extrapolated from a standard amplification curve obtained with the unconjugated **SCR** aptamer, and the conjugation efficiency was calculated as pmoles of aptamer conjugated/aptamer total (%). Three independent experiments were performed.

Cell culture

Human MDA-MB-231 and BT-549 TNBC and BT-474 Luminal B/HER2-positive breast cancer cell lines were purchased from the American Type Culture Collection (ATCC, Manassas, VA) and cultured as previously described.[22] *cis*-Pt-R cells, chronically resistant to cisplatin, were generated through prolonged exposure of MDA-MB-231 cells to the drug and grown as previously reported.[31] All cells were maintained under a 95% air/5% CO$_2$ atmosphere at 37 °C.

Cytotoxicity assay

Cytotoxicity evaluation of **RCDs** and **RCDs@Alg**, either unconjugated or conjugated with **sTN58** or **SCR** aptamers, was performed using thiazolyl blue tetrazolium bromide (MTT, AppliChem GmbH, Darmstadt, Germany) assay on MDA-MB-231 cells. Briefly, 5.0×10^3 cells per well, seeded in 96-well plates, were treated with different concentrations (50, 100, and 200 μg mL^{-1}) of the nanoformulations for 48 hours and cell viability was assessed following the manufacturer's protocol.

Confocal microscopy

MDA-MB-231, BT-549, *cis*-Pt-R or BT-474 cells (8.0×10^4 cells per well in 24-well), previously seeded on a coverslip for 24 hours, were incubated with **RCDs** or **RCDs@Alg**, either unconjugated or aptamer-conjugated, diluted to a final concentration of 100 μg mL^{-1} (**RCDs**) or 50 μg mL^{-1} (**RCDs@Alg**) in culture medium, from 10 up to 180 minutes. After three washes with Dulbecco's phosphate buffered saline (DPBS), the cells were fixed with 4% paraformaldehyde in DPBS for 30 minutes and subsequently incubated with Wheat Germ Agglutinin conjugated to Alexa Fluor 488 (WGA-488, Invitrogen, Carlsbad, CA) for 20 minutes at room temperature to visualize the cell membrane. Finally, after three washes with DPBS, the cells were incubated with 1.5 μM 4′,6-diamidino-2-phenylindole (DAPI, D9542, Sigma-Aldrich) and mounted with a glycerol/DPBS solution. Samples were visualized using a Zeiss LSM 700 META confocal microscope equipped with a Plan-Apochromat 63×/1.4 Oil DIC objective.
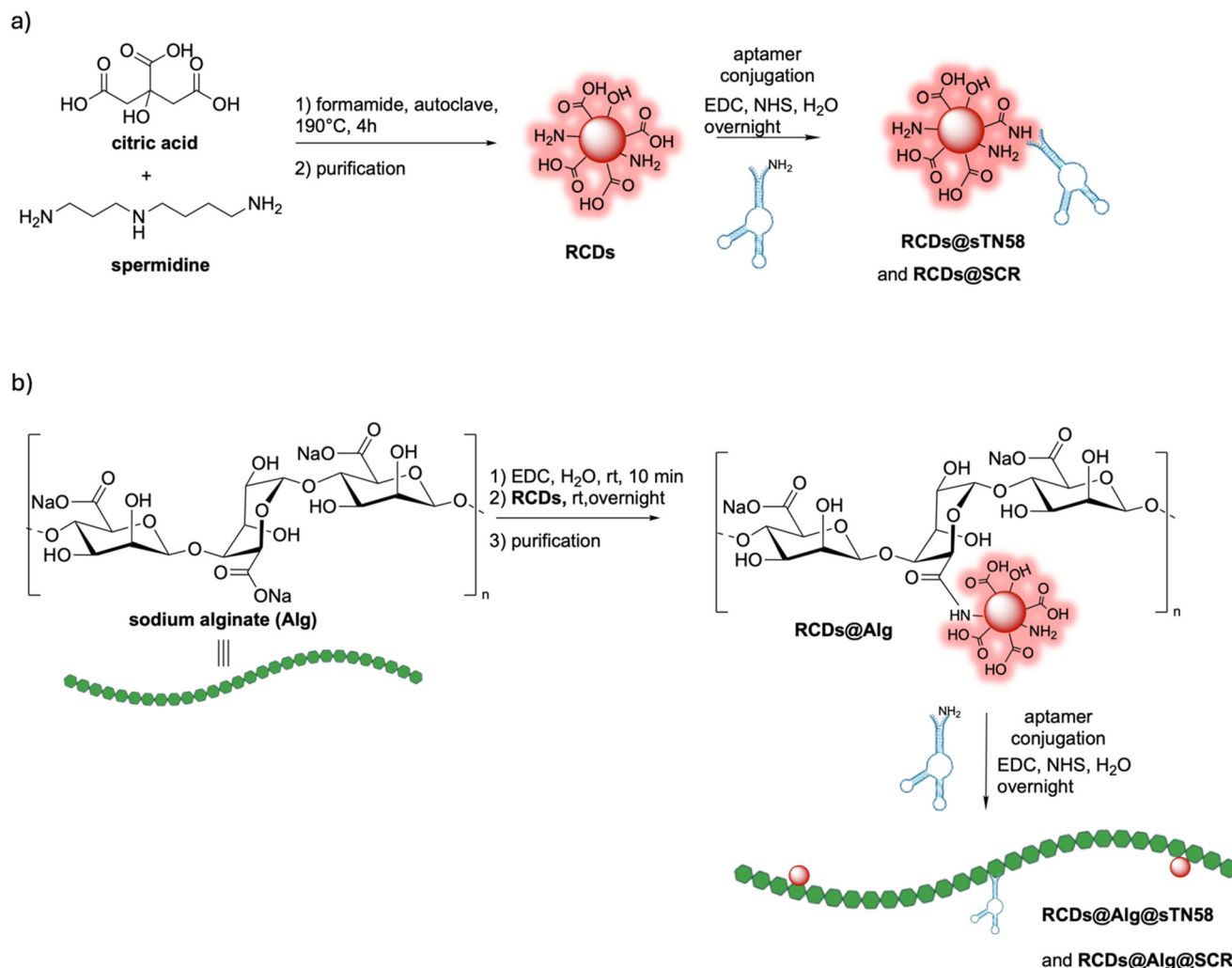
Photothermal experiments

Photothermal experiments were performed using an FC-808 fiber coupled laser system (CNI Optoelectronics Tech) in the continuous-wave operation mode at 808 nm with different laser powers. An optical lens was used to focus the continuous-wave diode light on a quartz cuvette (size: 1 × 1×3 cm) with a spot size of 8 mm. Control (DI water) and NP suspension with 4 different concentrations (0.1–3 mg mL^{-1}) were irradiated with a NIR laser (λ = 808 nm) at P = 1, 2 and 3 W cm^{-2} for 5 minutes. The temperature of the suspension (volume = 1 mL) was measured with a thermocouple (J-type Teflon) that was immersed in the suspension and connected to a computer for real-time data collection.

Results and discussion

Synthesis

According to our recently published procedure,[14] we synthesized **RCDs** through a solvothermal method by heating a solution of citric acid and spermidine in formamide at 190 °C (Scheme 1a). After a careful purification procedure involving filtration and precipitation, the **RCDs** were obtained as a dark red powder, and they were fully characterized with ATR-FTIR, TEM, UV-vis and spectrofluorimetric analysis. The synthesized nanoparticles were confirmed to show a bright red emission and to carry both carboxylic and amino groups on their

Scheme 1 (a) Synthesis of **RCDs** and their conjugation to the aptamers (**RCDs@sTN58** and **RCDs@SCR**). (b) Synthetic route to **RCDs@Alg**, **RCDs@Alg@sTN58** and **RCDs@Alg@SCR**.

surface, allowing the formation of covalent bonds with different derivatives.

Some of the obtained **RCDs** were employed for the decoration of sodium alginate (**Alg**) that, after activation of some of its carboxylic groups with EDC, formed amidic bonds with the amino groups present on the carbon dots' surface (Scheme 1b), yielding **RCDs@Alg** after dialysis purification.

Afterwards, the conjugation of the aptamer **sTN58** to the **RCDs@Alg** system was carried out: the dialyzed solution of **RCDs@Alg** in water was reacted with EDC and NHS and, after 10 minutes, the activated aptamer **sTN58** (1 µL of a 133 pmol µL^{-1} solution) was added, and the reaction mixture was left to stir at room temperature overnight. The ability of aptamers to recognize target cells is so powerful that the conjugation of a tiny amount is sufficient to obtain working systems. The obtained system **RCDs@Alg@sTN58** was purified by dialysis against distilled water for 24 hours. The same procedure was used for the non-related scrambled aptamer (**SCR**), for control experiments, to obtain **RCDs@Alg@SCR**. The amount of

aptamer conjugated to **RCDs@Alg** was evaluated by RT-qPCR analysis on **RCDs@Alg@SCR**. We calculated 5.6 pmol aptamer (corresponding to 0.07 pmol mg^{-1} dry matter) with a conjugation efficiency of 4.2%, which is comparable to what we calculated with the same aptamer conjugated through EDC/NHS on different types of nanoparticles.[28,29]

As a control, another portion of the synthesized **RCDs** was further directly functionalized with **sTN58** and **SCR** following a similar synthetic strategy: the activation of the carboxylic groups on the **RCD** surface with EDC and NHS allows conjugation with the amino group of the aptamer to yield **RCDs@sTN58** and **RCDs@SCR** systems, following the strategy depicted in Scheme 1a.

Characterization

The obtained systems were characterized with different techniques, which confirmed their structure and properties.

The ATR-FTIR spectrum of the red-brown powder of **RCDs** confirmed the presence of various functional groups on their

surface, together with the aromatic core responsible for their optical properties (Fig. 1, blue line). The pronounced bands in the 3150–3000 cm^{-1} range can be attributed to the stretching of N–H and O–H occurring in amino, alcohol and carboxylic groups; the peaks around 1700–1680 cm^{-1} and 1400 cm^{-1} were due to the stretching frequency of carboxylic derivatives on the **RCD** surface and the shoulder around 1300 cm^{-1} can be ascribed to C–N stretching.

The FT-IR of the **RCDs@Alg** system (Fig. 1, red line) resembled that of the pristine sodium alginate (**Alg**, Fig. 1, orange line), containing hydroxyl and carboxylate groups (3500–3000 cm^{-1} and 1600–1400 cm^{-1} ranges, respectively); the peaks related to the **RCDs** are difficult to identify probably owing to the relatively small number of nanoparticles' functional groups compared to those of the biopolymer. Two peak shoulders around 1698 cm^{-1} and 1460 cm^{-1} appeared in the functionalized alginate **RCDs@Alg** and can be ascribed to the formation of an amidic bond between **Alg** and **RCDs** (Fig. 1b, enlarged part). The amount of **sTN58** linked to both the **RCD** and **RCDs@Alg** systems was so low that any further signal could not be appreciated in the IR spectra.
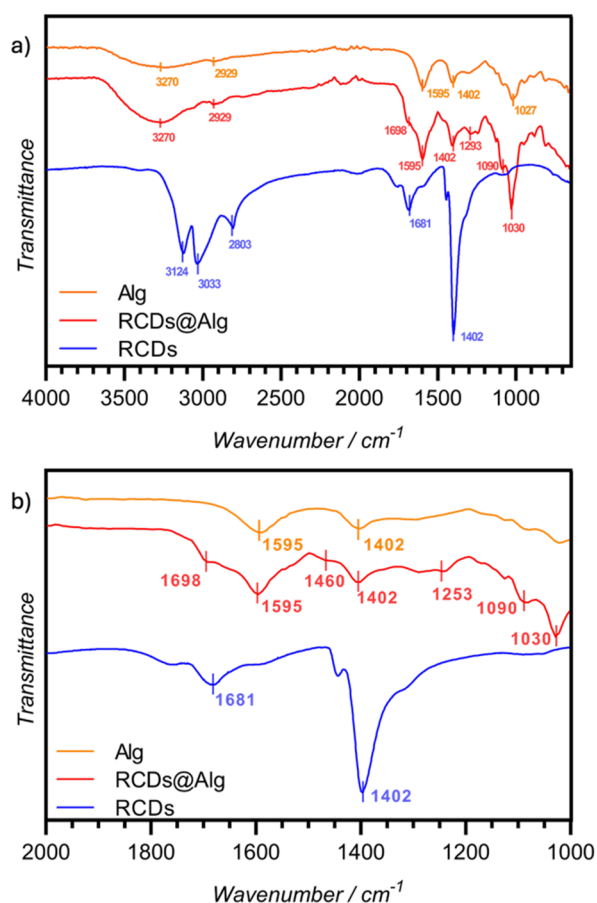
Then, the zeta-potentials of the fluorescent **RCDs** and the synthesized derivatives were measured in water at pH = 7 obtaining their respective surface charges. The presence of carboxylic groups that are deprotonated at neutral pH (COO$^-$) was confirmed by the negative surface charge (−30.4 mV) of **RCDs** (Table 1, entry 1). Accordingly, the zeta-potential of **RCDs@Alg** was found to be more negative, *i.e.* −44.9 mV (Table 1, entry 2), owing to the presence of the carboxylate groups in the alginate structure, with a consequent decrease in the negative surface charge. As expected, the conjugation of **sTN58** to both **RCDs@Alg** and **RCDs** slightly increased the value of the surface charge, as reported in Table 1 entries 3 and 4, due to the large number of negatively charged phosphate groups of the oligonucleotide.

Dimensional characterization was performed by TEM analysis. The **RCDs** were quite monodisperse nanoparticles (Fig. 2a) with an average diameter of about 4.16 nm (SD = 1.03, Fig. 2b). After functionalization with **RCDs** and the aptamer, the alginate structure remains almost unaffected and the presence of the nanoparticles is hard to identify, probably due to the carbon-based structure of all the components (Fig. 2c and S1). Also in this case, the functionalization with the aptamer did not cause significant changes in the morphology of the system.

The optical properties of the obtained systems were then evaluated through UV-vis absorption and photoluminescence emission in H$_2$O (Fig. 3).

Table 1 *Z*-potential values of the synthesized systems

Entry	System	*Z*-Potential
1	**RCDs**	−30.4 mV
2	**RCDs@Alg**	−44.9 mV
3	**RCDs@Alg@sTN58**	−52.9 mV
4	**RCDs@sTN58**	−32.9 mV

Fig. 1 ATR-FTIR spectra of **Alg** and the synthesized systems **RCDs** and **RCDs@Alg**: (a) full spectrum and (b) zoomed-in view of the 1000–2000 cm^{-1} range.
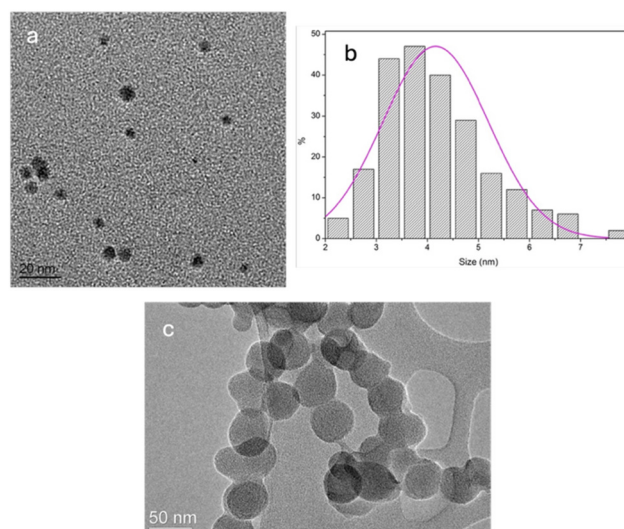

Fig. 2 TEM image of (a) **RCDs**, (b) their size distribution (calculated on 175 nanoparticles) and (c) **RCDs@Alg@sTN58**.

The properties of the original **RCDs** were substantially maintained in all further functionalization. The UV-vis absorption spectra of **RCDs** and **RCDs@Alg** displayed strong absorption throughout the visible region, even after the aptamer linkage. They showed a maximum peak in the UV region around 350–360 nm, probably due to the p–p* transition of the graphitic sp^2 domain, and broadened absorbance in the 450–620 nm range with a broad peak at around 540 nm that can be ascribed to the n/p* transition of aromatic and heteroaromatic systems (Fig. 3a).

As earlier observed,[14] the **RCDs**' emission maximum depended on the excitation wavelength, and it proved to be red shifted by increasing λ_{exc}. According to our previous results, excitation at 540 nm resulted in the best compromise between the emission intensity and its energy; therefore, we also evaluated the fluorescence of the new systems excited at 540 nm. As reported in the normalized graph in Fig. 3b, the emission of both **RCDs@Alg** and **RCDs@Alg@sTN58** showed a slight red shift compared to the starting **RCDs** (around 625 *versus* 620 nm) while the emission of **RCDs@sTN58** remained substantially unaffected after the conjugation of the aptamer to **RCDs**.
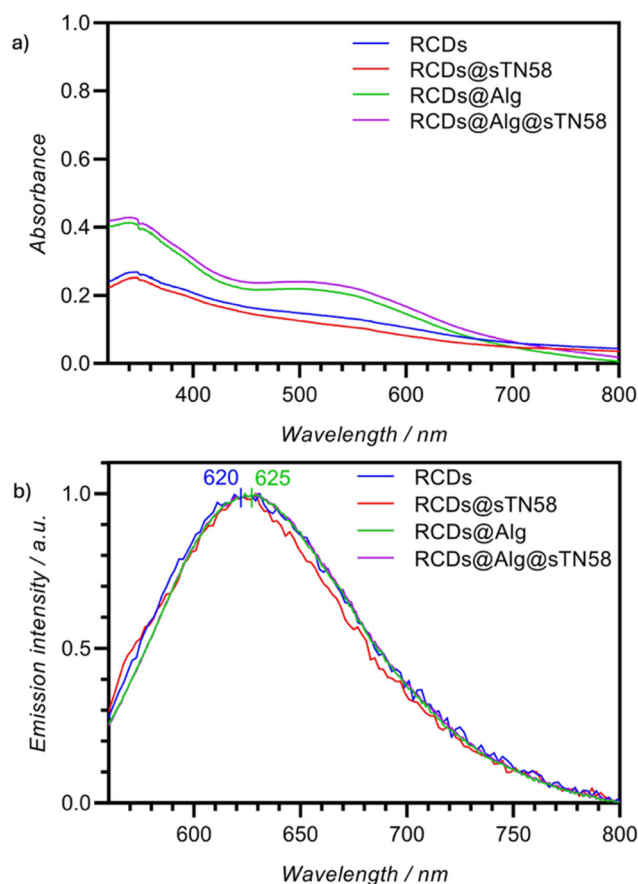
The stability of **RCDs@Alg@sTN58** in PBS 1× (at a concentration of 0.1 mg ml^{-1}) buffer solution mimicking the biological environment was assessed by monitoring their properties over time. The absorbance and emission spectra remained almost unaffected after 72 h (Fig. S2), as did the *Z*-potential (Fig. S3), and the samples did not present any agglomeration (Fig. S4), suggesting good stability of the system.

Uptake analysis in TNBC cells

To evaluate the **sTN58**-mediated **RCD** delivery to TNBC cells, the human CD44-positive mesenchymal stem-like (MES) MDA-MB-231 and BT-549 cell lines and the cisplatin-resistant MDA-MB-231 derivative (*cis*-Pt-R) were used as target cells. We previously showed that **sTN58** efficiently internalizes into these cell lines, *via* CD44 recognition, both in its free form[22,32] and when conjugated to polymeric nanoparticles.[23] Thus, we first verified that **RCDs** and **RCDs@Alg** systems, equipped with either **SCR** or **sTN58**, when incubated for 48 hours at 37 °C on TNBC cells have no adverse effects on cell viability at concentrations up to at least 200 μg mL^{-1} (Fig. 4).

Next, the fluorescence emitted from the unconjugated and aptamer-conjugated **RCDs** was collected by confocal microscopy of MDA-MB-231 cells treated with the nanoparticles at 37 °C for 30 minutes. As shown (Fig. 5a), the signal associated with the untargeted **RCDs** was nearly undetectable,
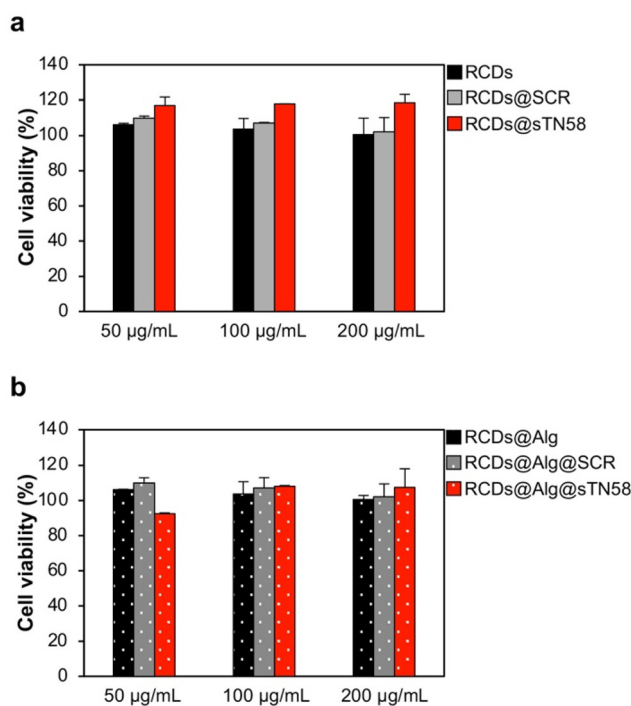
Fig. 3 (a) Absorbance and (b) normalized emission properties of the synthesized systems **RCDs**, **RCDs@sTN58**, **RCDs@Alg** and **RCDs@Alg@sTN58**.

Fig. 4 Cytotoxicity evaluation of **RCD** and **RCDs@Alg** systems. MDA-MB-231 cells were treated with the indicated concentrations of **RCDs**, **RCDs@SCR** or **RCDs@sTN58** (a) and **RCDs@Alg**, **RCDs@Alg@SCR** or **RCDs@Alg@sTN58** (b) for 48 hours, and their viability was measured with the MTT assay. Results are presented as percentages relative to untreated control cells. Bars depict means ± SD (*n* = 3).
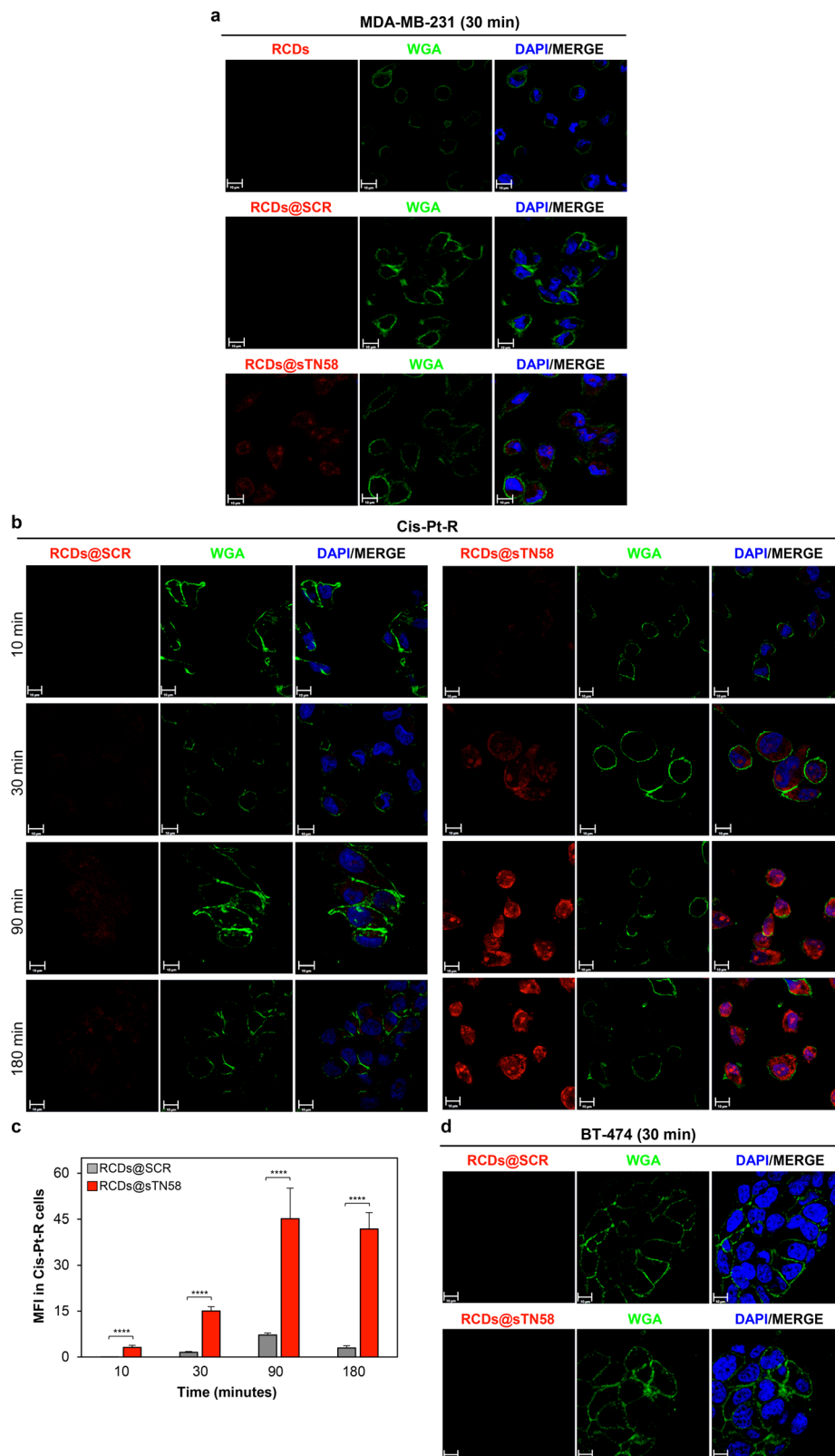
Fig. 5 Selective uptake of **RCDs@sTN58** in TNBC cells. (a, b, and d) Representative confocal images of MDA-MB-231 (a), *cis*-Pt-R (b) and BT-474 (d) cells treated with **RCDs**, **RCDs@SCR** or **RCDs@sTN58** at 37 °C for the indicated times. After washing and fixation, the cells were labelled with WGA (green) to visualize the cell membrane and with DAPI (blue) to stain nuclei. **RCD** systems are displayed in red. Magnification: 63×, 1.0× digital zoom, scale bar = 10 μm. All digital images were captured under the same settings to enable a direct comparison of staining patterns. (c) Mean fluorescence intensity (MFI) of **RCDs@SCR** or **RCDs@sTN58** in *cis*-Pt-R cells was evaluated using Zeiss software on a minimum of 50 cells for each sample. Bars depict means $\pm$ SD (n = 3). ****P < 0.0001 relative to **RCDs@SCR**; Student's *t*-test.

whereas the **RCDs@sTN58** signal was clearly visible and accumulated beneath the cell membrane and within the nuclei, indicating that **sTN58** effectively promotes cellular uptake of **RCDs**. These findings were reproduced in *cis*-Pt-R cells (Fig. 5b), consistent with the **sTN58** selective targeting of CD44, which is overexpressed in chemoresistant cells.[22] As shown, **RCDs@sTN58** exhibited a time-dependent cellular uptake profile, with intracellular fluorescence intensity increasing over time and reaching a plateau at 3 hours (Fig. 5c). As expected, no signal was observed in CD44-negative non-TNBC BT-474 cells (Fig. 5d).

Importantly, similar results were observed with the sodium alginate–RCD systems, which were efficiently incorporated by **sTN58** into MDA-MB-231 (Fig. 6), BT-549 (Fig. S5a) and *cis*-Pt-R (Fig. S5b) target cells, but not into BT-474 control cells (Fig. S5c), indicating that alginate readily supports aptamer attachment for active targeting. Notably, the facile surface functionalization and high surface area will allow the use of our aptamer–alginate–RCD system as an ideal scaffold for the co-loading of therapeutic agents, enabling combination therapy for TNBC.

Finally, we tested whether our **RCD**-based systems could be used as photothermal agents. Four different concentrations of **RCDs** (0.1–3 mg mL^{-1}) in water were irradiated with laser

Table 2 Temperature increase after laser irradiation of RCD-containing samples. 1 mL of each sample was irradiated with a NIR laser (λ = 808 nm) at P = 1, 2 and 3 W cm^{-2} for 5 minutes, and the suspension temperature was monitored using a thermocouple. The concentration of RCDs in water was varied between 0.1 and 3 mg mL^{-1}, while in the case of **RCDs@Alg**, it was 0.5 mg mL^{-1}

Sample (mg mL^{-1})	ΔT at 1 W	ΔT at 2 W	ΔT at 3 W
RCDs (0.1)	0.9	2.3	4.9
RCDs (0.5)	2.3	5	10.7
RCDs (1)	3.7	8.7	14.4
RCDs (3)	9.3	20.2	31.9
Alg (0.5)	0.9	2	3.1
RCDs@Alg (0.5)	3	7.1	12.3

power (P) = 1, 2 and 3 W cm^{-2} for 5 minutes. The results are reported in Table 2. Interestingly, **RCDs** demonstrated good hyperthermia generation, with an expected profile where the hyperthermia effect increases by increasing either the concentration of the absorbing species (**RCDs** from 0.1 to 3 mg mL^{-1}) or the power density (from 1 to 3 W cm^{-2}). Expectedly, the most prominent heating was achieved at higher concentrations and higher laser power (ΔT = 31.9 °C at 3 mg mL^{-1} and P = 3 W cm^{-2}). However, for therapeutic purposes, a ΔT of 5 °C is sufficient to reach the mild hyperthermia region (41–43 °C) to sensitize cells for other therapies and avoid thermal ablation (>50 °C).[33] In our case, this can be achieved already with the lowest tested **RCD** concentration (0.1 mg mL^{-1}) (ΔT = 4.9 °C at P = 3 W cm^{-2}) or with an intermediate concentration of 0.5 mg mL^{-1} at only 2 W cm^{-2}, which indicates the good therapeutic potential of the developed nanoparticles. Since the concentration of 0.5 mg mL^{-1} is reasonable for future *in vitro* and *in vivo* therapeutic attempts, we decided to irradiate the suspensions of pure **Alg** as the control and **RCDs@Alg** at a 0.5 mg mL^{-1} concentration. Interestingly, **Alg** only reached a ΔT of up to 3 °C even at higher power density, while **RCDs@Alg** reached 12.3 °C at P = 3 W cm^{-2} and 7.1 °C at P = 2 W cm^{-2} indicating promising potential for hyperthermia applications. Importantly, no change in the absorption spectra before and after laser irradiation was observed (Fig. S6 and S7), indicating that no photo-induced degradation occurred, which is a very important feature in comparison with metallic nanosystems, where reshaping phenomena are often observed under irradiation.

Fig. 6 Selective uptake of **RCDs@Alg@sTN58** in MDA-MB-231 cells. Representative confocal images of MDA-MB-231 cells incubated with **RCDs@Alg**, **RCDs@Alg@SCR** or **RCDs@Alg@sTN58** for 30 minutes at 37 °C. **RCDs@Alg** systems, WGA (cell surface) and DAPI (nuclei) are visualized in red, green, and blue, respectively. Magnification: 63×, 1.0× digital zoom, scale bar = 10 μm. All digital images were captured under the same settings to enable a direct comparison of staining patterns.

Conclusions

In conclusion, we have developed an advanced surface-engineered platform based on carbon nanodots coated with biocompatible alginate and functionalized with a selective aptamer targeting triple-negative breast cancer (TNBC) cells. The alginate coating ensures excellent biocompatibility and provides reactive sites for stable aptamer conjugation. *In vitro* results demonstrate that these nanodots selectively recognize TNBC cell lines over scrambled oligonucleotide controls. Moreover,
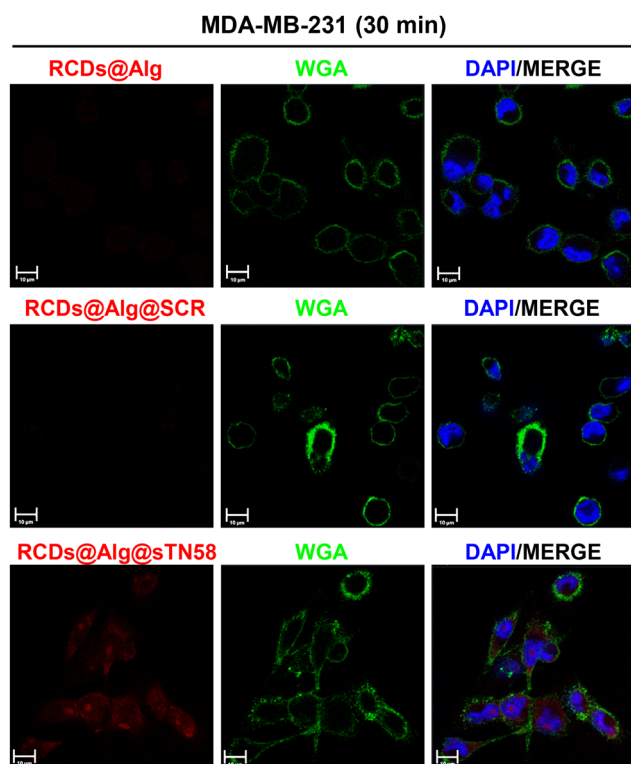
preliminary data indicate their potential as nanoheaters for future photothermal therapy applications.

This multifunctional system combines targeted recognition with the prospect of therapeutic action. Further *in vivo* pre-clinical studies are needed to assess the efficacy, safety, and potential toxicity of our nanosystems, which are essential steps for their future translational development.

Overall, our approach provides a promising tool for selective cancer targeting.

Author contributions

L. S. and L. C. planned and supervised the project. S. M., A. C., N. K., S. T. and L. A. provided all the experimental procedures. L. S., N. K. and L. C. prepared the original draft. M. C. F, E. L. and S. C. reviewed the manuscript and provided structural characterization.

Conflicts of interest

There are no conflicts to declare.

Data availability

The data supporting this article have been included as part of the supplementary information (SI). Supplementary information: TEM analysis, absorbance and emission spectra in buffer solution, Z-potentials, pictures of buffer solutions, cellular uptake and cell line specificity, and absorbance spectra before and after laser irradiation. See DOI: https://doi.org/10.1039/d5bm01297j.

Acknowledgements

References

1 https://www.who.int/news-room/fact-sheets/detail/cancer.
2 C.-L. Shen, H.-R. Liu, Q. Lou, F. Wang, K.-K. Liu, L. Dong and C.-X. Shan, *Theranostics*, 2022, **12**, 2860–2893.
3 X. Xu, R. Ray, Y. Gu, H. J. Ploehn, L. Gearheart, K. Raker and W. A. Scrivens, *J. Am. Chem. Soc.*, 2004, **126**, 12736–12737.
4 H. Singh, M. Razzaghi, H. Ghorbanpoor, A. Ebrahimi, H. Avci, M. Akbari and S. Hassan, *Adv. Drug Delivery Rev.*, 2025, **224**, 115644.
5 J. Wang, Yu Fu, Z. Gu, H. Pan, P. Zhou, Qi Gan, Y. Yuan and C. Liu, *Small*, 2024, **20**, 2303773.
6 M. Bartkowski, Y. Zhou, M. N. A. Mustafa, A. J. Eustace and S. Giordani, *Chem. – Eur. J.*, 2024, **30**, e202303982.
7 J. Liu, R. Li and B. Yang, *ACS Cent. Sci.*, 2020, **6**, 2179–2195.
8 M. Alafeef, I. Srivastava, T. Aditya and D. Pan, *Small*, 2024, **20**, 2303937.
9 Z. Bian, E. Gomez, M. Gruebele, B. G. Levine, S. Link, A. Mehmood and S. Nie, *Chem. Sci.*, 2025, **16**, 4195.
10 M. L. Liu, B. B. Chen, C. M. Li and C. Z. Huang, *Green Chem.*, 2019, **21**, 449–471.
11 W. Qin, M. Wang, Y. Li, L. Li, K. Abbas, Z. Li, A. C. Tedesco and H. Bi, *Mater. Chem. Front.*, 2024, **8**, 930.
12 K. Warjurkar, S. Pandab and V. Sharma, *J. Mater. Chem. B*, 2023, **11**, 8848–8865.
13 Y. Jiang, T. Zhao, W. Xu and Z. Peng, *Carbon*, 2024, **219**, 118838.
14 S. Maturi, A. Baschieri, E. Locatelli, M. Buccioli, M. Comes Franchini and L. Sambri, *Nanoscale Adv.*, 2025, **7**, 448–455.
15 Y. Ren, Q. Wang, W. Xu, M. Yang, W. Guo, S. He and W. Liu, *Int. J. Biol. Macromol.*, 2024, **279**, 135019.
16 T. Fazal, B. N. Murtaza, M. Shah, S. Iqbal, M. Rehman, F. Jaber, A. A. Dera, N. S. Awwad and H. A. Ibrahium, *RSC Adv.*, 2023, **13**, 23087.
17 K. Y. Lee and D. J. Mooney, *Prog. Polym. Sci.*, 2012, **37**, 106–126.
18 S. N. Pawar and K. J. Edgar, *Biomaterials*, 2012, **33**, 3279–3305.
19 L. Agnello, S. Camorani, M. Fedele and L. Cerchia, *Explor. Target. Antitumor Ther.*, 2021, **2**, 107–121.
20 S. Shigdar, L. Agnello, M. Fedele, S. Camorani and L. Cerchia, *Pharmaceutics*, 2021, **14**, 28.
21 G. Bianchini, C. De Angelis, L. Licata and L. Gianni, *Nat. Rev. Clin. Oncol.*, 2022, **19**, 91–113.
22 A. Caliendo, S. Camorani, L. E. Ibarra, G. Pinto, L. Agnello, S. Albanese, A. Caianiello, A. Illiano, R. Festa, V. Ambrosio, G. Scognamiglio, M. Cantile, A. Amoresano, M. Fedele, A. Zannetti and L. Cerchia, *Bioact. Mater.*, 2025, **50**, 443–460.
23 L. E. Ibarra, S. Camorani, L. Agnello, E. Pedone, L. Pirone, C. A. Chesta, R. E. Palacios, M. Fedele and L. Cerchia, *Pharmaceutics*, 2022, **14**, 626; Erratum in: L. E. Ibarra, S. Camorani, L. Agnello, E. Pedone, L. Pirone, C. A. Chesta, R. E. Palacios, M. Fedele and L. Cerchia, *Pharmaceutics*, 2024, **16**, 1281.
24 Y. Shi, X. Yanga, Y. Zhang and S. Lu, *Carbohydr. Polym.*, 2025, **351**, 123112.
25 F. Oudjedi and A. G. Kirk, *NanoSelect*, 2025, **6**, e202400107.
26 Y. Cai, T. Chai, W. Nguyen, J. Liu, E. Xiao, X. Ran, Y. Ran, D. Du, W. Chen and X. Chen, *Signal Transduction Targeted Ther.*, 2025, **10**, 115.
27 T. Zhang, J. Wu, Z. Tang and S. Qu, *Mater. Chem. Front.*, 2023, **7**, 2359–2372.
28 I. Monaco, S. Camorani, D. Colecchia, E. Locatelli, P. Calandro, A. Oudin, S. Niclou, C. Arra, M. Chiariello,

L. Cerchia and M. Comes Franchini, *J. Med. Chem.*, 2017, **60**, 4510–4516.

29 S. Camorani, A. Caliendo, E. Morrone, L. Agnello, M. Martini, M. Cantile, M. Cerrone, A. Zannetti, M. La Deda, M. Fedele, L. Ricciardi and L. Cerchia, Bispecific aptamer-decorated and light-triggered nanoparticles targeting tumor and stromal cells in breast cancer derived organoids: implications for precision phototherapies, *J. Exp. Clin. Cancer Res.*, 2024, **43**, 92.

30 C. Venegoni, S. Tortorella, A. Caliendo, I. Locatelli, A. D. Coste, E. Locatelli, F. Capancioni, E. Bua, S. Camorani, A. Salonia, F. Montorsi, J. Jose, M. Moschini, L. Cerchia, M. Comes Franchini and M. Alfano, *Adv. Healthcare Mater.*, 2025, **14**, e2403314.

31 S. Camorani, I. Granata, F. Collina, F. Leonetti, M. Cantile, G. Botti, M. Fedele, M. R. Guarracino and L. Cerchia, *iScience*, 2020, **23**, 10097.

32 S. Camorani, A. d'Argenio, L. Agnello, R. Nilo, A. Zannetti, L. E. Ibarra, M. Fedele and L. Cerchia, *Int. J. Mol. Sci.*, 2022, **23**, 3511.

33 G. C. van Rhoon, M. Franckena and T. L. M. Ten Hagen, *Adv. Drug Delivery Rev.*, 2020, **163–164**, 145–156.